Label-free analysis of gingival crevicular fluid (GCF) by surface enhanced Raman scattering (SERS)†

Stefano Fornasaro, *[a] Federico Berton,[b] Claudio Stacchi,[b] Federica Farina,[b] Alessandro Esposito,[a] Valter Sergo,[a,c] Roberto Di Lenarda[b] and Alois Bonifacio [a]

Gingival crevicular fluid (GCF) is an interesting biofluid reflecting the physiological and pathological states of a single dental element. Due to this unique feature, in recent years, metabolomic analysis of GCF has gained attention as a biometric tool for the diagnosis and therapy of periodontal disease. Traditional methods are, however, too slow, cumbersome and expensive for a health-care routine. Surface enhanced Raman scattering (SERS) can offer rapid and label-free detailed molecular fingerprints that can be used for biofluid analysis. Here we report the first SERS characterization of GCF using an easy and quick sample preparation. The dominant features in the SERS spectrum of GCF are ascribed to very few metabolites, in particular to uric acid, hypoxanthine, glutathione and ergothioneine. Additionally, we succeeded in differentiating between the SERS signal of GCF collected from healthy volunteers and the one collected from patients with periodontal disease.

Introduction

Gingival crevicular fluid (GCF) was first recognized in 1899 as an oral cavity-specific biofluid that emerges between the surface of the tooth and the sulcular epithelium.[1] Small amounts of GCF are reportedly present in healthy periodontium, whereas big amounts are observed in inflamed or mechanically stimulated periodontal tissues.[2] The biochemical composition of GCF is similar to that of blood serum and includes immunoglobulins, peptides, enzymes, local mediators, toxic cells and products of tissue breakdown as well as those from supra- and subgingival bacteria.[3,4] Given the highly localized accumulation of GCF, the analysis of the composition of this fluid enables the determination of dental biomarkers at specific sites in the dentition (*i.e.*, assaying for abnormalities in levels of dental biomarkers for a particular dental element).[5]

Recently, metabolomic analysis of GCF has gained attention for the diagnosis and treatment of periodontal disease,[6,7] one of the most common diseases affecting the dental elements, ranging from the earliest stage of marginal gingivitis to the most advanced destructive periodontitis.[8–11] Untargeted metabolomics approaches (*i.e.* the simultaneous measurement of multiple metabolites in a biological sample) have been proposed to distinguish the biochemical signature of individuals with periodontal disease from that of healthy individuals and to discriminate between various stages and progression of periodontal disease.[12,13] However, high-throughput mass spectrometry (MS) based analyses are too slow, cumbersome and expensive for a health-care routine. Thus, versatile, cost-effective and fast alternatives for performing metabolic profiling of GCF are required.

Surface-enhanced Raman scattering (SERS) is a spectroscopic technique that employs metal nanostructures (*i.e.* the SERS substrate) for amplifying the Raman signal of analytes of interest. In label-free SERS, each spectrum contains information about the molecules that freely adsorb onto the substrate surface, driven by the affinity with the surface itself.[14] In the last decade, SERS has emerged as one of the most attractive and powerful techniques for the identification of the biochemical profile of biofluids.[15,16] Containing information mainly about low-molecular-weight metabolites, SERS spectra of biofluids provide a "biochemical snapshot" of potentially clinically relevant information about the metabolic status of a sample at the moment of analysis. Different from other metabolomic approaches, SERS can be performed by minimally

[a]*Raman Spectroscopy Lab, Department of Engineering and Architecture, University of Trieste, 34100 Trieste, Italy. E-mail: sfornasaro@units.it*
[b]*Department of Medical, Surgical and Health Sciences, University of Trieste, 34100 Trieste, Italy*
[c]*Faculty of Health Sciences, University of Macau, SAR Macau, China*
†Electronic supplementary information (ESI) available. See DOI: 10.1039/d0an01997f

trained personnel, with relatively inexpensive instrumentation and without complex sample preparation. Several works report SERS analysis of serum,[17–19] plasma,[20,21] and saliva,[22] in which SERS spectra were shown to display characteristic spectral features in the case of patients with specific diseases, such as cancer or autoimmune diseases. In one work by d'Apuzzo *et al.*,[23] SERS spectra of extracted GCF were used to monitor different phases of orthodontic treatment. However, no SERS study has yet focused on GCF in the context of metabolomics.

The aim of the present study was to demonstrate the feasibility of the SERS approach for a fast, sensitive and specific characterization of the GCF metabolic profile, using the simplest collection technique and a compact and portable instrument. Additionally, we succeeded in differentiating between the SERS signal of GCF collected from healthy volunteers and the one collected from patients with a confirmed diagnosis periodontitis and gingivitis. To the best of our knowledge, this is the first SERS study on GCF profiling of the biochemical perturbations that accompany periodontal disease.

Experimental

Materials and reagents

All chemicals (analytical grade) were purchased from Merck (Darmstadt, Germany) and used as received. Ultrapure deionized (DI) water of 18.2 MΩ cm resistivity at 25 °C was used throughout the experiments and it was obtained using a Millipore Milli-Q system (Merck, Germany). Methylcellulose GCF collection strips (Periopaper®) were purchased from Oraflow Inc. (NY, USA).

Synthesis and characterization of silver colloids

Colloidal aqueous dispersions of Ag nanoparticles (Ag-NPs) were synthesized according to the protocols adapted from Lee–Meisel.[24] Briefly, $AgNO_3$ (45 mg) was dissolved in 250 mL of DI water and heated to boiling. 5 mL of 1% (wt/v) aqueous sodium citrate tribasic solution were then added dropwise to the $AgNO_3$ solution under vigorous magnetic stirring. The reaction mixture was then left under stirring on a steady boil for 1 h. The reaction was deemed to have reached its endpoint once the solution had a milky green hue. All glassware used for the preparation of Ag-NPs was carefully cleaned with a NoChromix® mixture and concentrated solutions of strong acids (HNO_3), and then thoroughly rinsed with DI water. The method was replicated for the synthesis of three batches of Ag-NPs. The successful synthesis of the produced Ag-NPs was confirmed by UV-Vis spectroscopy, using a Cary 60 UV-Vis spectrometer (Agilent Technologies). An absorption/extinction spectrum was obtained over a range of 300 to 800 nm. The values of the extinction band maxima (403–406 nm) were consistent with the values previously reported in the literature for Ag-NPs synthesized using the same method (Fig. S1†). Ag-NP batches were stored in the dark at room temperature and were stable for several months.

GCF sample collection

GCF samples were provided by the Maxillofacial Surgery and Dental Department of University Hospital Giuliano-Isontino of Trieste. Informed consent was obtained for any experiments with human subjects. The diagnosis was established based on a clinical examination according to the currently accepted definition of periodontitis and gingivitis,[10,25–27] taking into consideration also the Periodontal Screening and Recording (PSR). GCF samples were taken from the mesial or distal-vestibular aspect of 67 teeth from 13 patients (aged between 40 and 75 years, see Fig. S2†), according to the protocol reported by Papagerakis *et al.*[5] Before gingival crevicular fluid collection, the tooth was air-dried, any *iuxta* gingival plaque was gently removed manually and clean cotton rolls were inserted at the level of the vestibular fornix to isolate the tooth surfaces. Then, a Periopaper® strip was gently inserted 1 mm inside the gingival sulcus. Each strip remained in position for a total of 30 seconds before immediate removal. Any strips visibly contaminated with blood, pus or saliva were discarded. Following GCF collection, each strip was placed into its corresponding labelled 1.5 mL microfuge tube. Each tube was immediately placed at −4 °C and then transferred to a −80 °C freezer until analysis.

Sample preparation for SERS measurements

On the day of analysis, each strip was kept at room temperature, processed by adding a colloidal dispersion of Ag-NPs, centrifuged (10 min, 4289*g*), and allowed to dry at room temperature for about 15 minutes. To facilitate handling, all dried strips were placed on a standard microscope slide (25 × 75 mm) that was fitted onto the portable microscope stage before measurement.

Instrumentation and spectra collection

SERS spectra were recorded at room temperature (22 ± 0.5 °C) using a portable i-Raman Plus integrated system (BWS465-785S, B&W Tek, Newark, DE, USA). The instrument was equipped with a CleanLaze® 785 nm laser, tuned to deliver ~38 mW at the sample, on a spot of about 105 μm in diameter, through the BAC151B Raman Video Micro-sampling System mounting a 20× Olympus objective (working distance 8.8 mm, N.A. 0.25). Instrument settings were optimised to maximise the signal and avoid sample degradation arising from laser excitation. The spectral acquisition was performed using the BWSpec™ version 4.03_23_c (B&W Tek., Newark, DE, USA) software in the Raman shift range of 62–3202 cm^{-1}, with an average spectral resolution of 3.22 cm^{-1}, using a 10 s CCD exposure for a single accumulation. The BWSpec™ software allowed the collection of a background signal (dark) before data acquisition and its subtraction from the collected data. To compensate for intra-substrate variability, a total of 5 spectra were collected from different positions of the same substrate and were then averaged into one spectrum per sample. Wavenumber calibration was checked before and

during every data collection session by collecting a spectrum of paracetamol as a standard reference.

Data processing and visualization

All data processing and visualization were performed within the R software environment (version 4.0.1 – "See Things Now") for statistical computing and graphics, built on the packages hyperSpec[28] and baseline.[29] Annotated R scripts are available on GitHub (https://github.com/fornasaros/s4a). Spectral pre-processing consisted of three steps: (i) cropping spectral data to keep the Raman shifts between 400 and 1800 cm^{-1}; (ii) baseline correction and (iii) intensity vector normalization. For the baseline correction, a baseline obtained with an asymmetric least squares (AsLS) algorithm ($\lambda = 4$ and $p = 0.01$) was fit automatically to the whole spectral range and was subtracted from each spectrum of the dataset. Spectral fitting was obtained using a classic least squares regression of the median GCF spectrum using contributions from ergothioneine, uric acid, hypoxanthine, reduced glutathione (pure components) and naked Periopaper strip covered with Ag NPs (background). Normalized SERS spectra of 10 μM aqueous solutions of these metabolites were independently obtained for this purpose. Each GCF spectrum in the dataset was modelled as a sum of four reference spectra and the background (each scaled by a corresponding coefficient generated by the *nls* function from the *stats* package), following the method proposed by Lutz *et al.*[30] To evaluate the performance of the spectral fitting method, the lack of fit (Lof) explained variance (R^2) and relative fitting error (RFE) were calculated. Principal component analysis (PCA) was used as an exploratory method to visualize patterns among samples and to interpret signal features that characterize different groups, according to their label. Data were centred but not scaled prior to the PCA.

Results and discussion

SERS analysis of GCF

After Ag-NP addition, centrifugation and drying, intense spectra were observed directly from the methylcellulose strip covered with Ag NPs, without any further sample pre-treatments. Preliminary experiments were carried out to identify the best working conditions with regard to the reproducibility of the SERS signal from the CGF samples. 75 μL of colloid/sample and 10 minutes of centrifuge were identified as the best conditions to obtain a sufficiently stable and reproducible SERS signal, with a very good signal-to-noise ratio, and no visible background contribution from paper (Fig. 1a). The label-free SERS fingerprint of a complex mixture, such as GCF, might be considered as a superposition of SERS spectra of some of its pure constituents, depending on both the relative concentration of the involved species and their chemical affinity for the metal surface, the latter factor being the most relevant.[31] Despite significant differences in the biochemical composition, the dominant features in the GCF spectra were

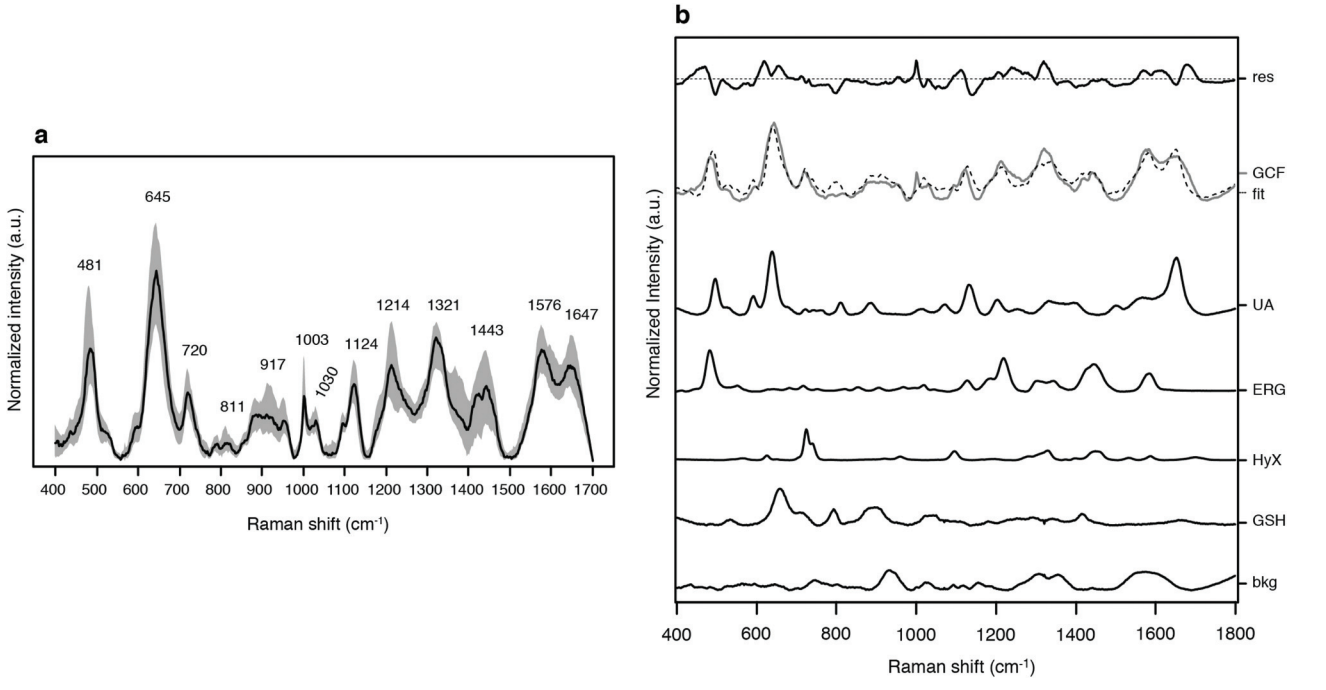

Fig. 1 (a) Median (solid lines) and interquartile (IQR) range (shaded areas) of the baseline-corrected and intensity-normalized SERS spectra of GCF samples. (b) Comparison of SERS spectra of GCF and some model compounds. The dashed line represents the best-fit spectrum (fit), *i.e.* the spectral sum of all components as displayed in this figure: UA, uric acid; ERG, ergothioneine; Hyp, hypoxanthine; GSH, glutathione; bkg, a naked Periopaper strip covered with Ag NPs. The best-fit spectrum was subtracted from the GCF spectrum to obtain the residuals (res). Lack-of fit = 4.67% (see the supplementary methods for details).

remarkably similar to the ones found in deproteinized biofluids, such as plasma, serum,[32,33] tears,[34] and saliva.[22] In light of these similarities, initial evidence suggesting the molecular origins of the label-free 785 nm excited SERS spectrum of GCF on Ag was provided by comparison of SERS spectra of GCF and aqueous solutions of some biomolecules, known to be responsible for the most intense bands in the SERS spectra of those biofluids (Fig. S2†). We have found that characteristic bands present in the GCF SERS spectral profile can be attributed to the vibrational modes of uric acid (bands centred at 645 and 1124 cm^{-1}), hypoxanthine (the band at 720 cm^{-1}), ergothioneine (bands centred at 481, 1214 and 1443 cm^{-1}), and the reduced form of glutathione (the band at 917 cm^{-1}). Interestingly, only minor spectral contributions from vibrational bands associated with aminoacidic aromatic residues and to peptide backbone vibrations (1003 cm^{-1}, Phe ring breathing; 1647 cm^{-1}, amide I[35]) can be identified. Thus, the SERS spectrum of GCF seems to be dominated by the bands of a small number of low-molecular-weight (*i.e.* <3 kDa) metabolites. This is remarkable, considering the high amount of proteins usually found in GCF (230 different proteins identified).[36] Apparently, such a set of low-molecular-weight metabolites interact more efficiently with metal nanostructures than proteins, in which only the aromatic amino acids are known to yield intense SERS spectra. To corroborate this interpretation, the SERS spectra of GCF were fit to a linear combination of the SERS spectra of uric acid, hypoxanthine, ergothioneine, and glutathione. The background signal of the paper strip covered with AgNPs (containing mainly contributions from the citrate used for colloid preparation) was also included. Such a method is rapid and easy to implement and offers satisfactory fitting results for qualitative evaluation. Both the wavenumbers and intensities can be seen to fit quite well. With a few exceptions (the bands at 1003 and 1321 cm^{-1}), nearly all major vibrational features and their relative intensities were captured by the fitting procedure (Fig. 1b), with an average lack-of-fit of 4.67% (see the ESI† for details). Differences in relative intensities between fitted spectra and the observed GCF spectra can be seen by looking at the residual profile. These differences, together with some systematic vibrational frequency shifts between the GCF and reference solutions spectra, are to be expected and can be attributed to the complexity of the GCF matrix, where interactions between many compounds (molecular complex formation) occur at the substrate surface,[14] influencing the affinity of the metabolites for the metal surface. This molecular crowding at the surface was unaccounted for in the fitting calculations. Moreover, the analysis of the residual profile can offer useful insights into other minor putative contributors to the SERS spectrum of GCF. The vibrational bands highlighted in the residual profile can be attributed to the sum of other GCF metabolites, not considered in the pure component set (*e.g.* xanthine and adenosine) that can be adsorbed onto the Ag surface. Furthermore, dedicated and focused studies, with the support of more powerful hyphenated techniques, such as HPLC/GC-MS, could possibly help in assigning all bands observed in SERS spectra of GCF to specific metabolites.

Interestingly, the GCF SERS spectra reported in the present work are quite different from those reported by d'Apuzzo *et al.*[23] We attribute such differences to the use of different metal substrates (Ag instead of Au nanoparticles) and different wavelengths used for excitation (785 instead of 633 nm) since SERS signals of the same analyte strongly depend on the type of metal surface and the choice of laser excitation wavelength.

GCF differentiation

We demonstrated that the dominant features in the SERS spectrum of GCF can be assigned to a handful of metabolites involved in the host response to oxidative stress and inflammation. Current results on the relationship between periodontal health and antioxidants are rather consistent; uric acid and reduced glutathione as specific antioxidants were reported to be significantly lower in the GCF of patients with chronic or aggressive periodontitis,[37,38] suggesting that the decreased activities of these antioxidants are associated with periodontitis. Moreover, Barnes *et al.* demonstrated how periodontal-disease-induced oxidative stress and inflammation are mediated through the purine demolition pathway, which is significantly accelerated at the disease sites.[39,40]

We therefore tried to differentiate the GCF collected from healthy dental elements from the GCF collected from dental elements with a periodontal disease diagnosis, on the basis of its SERS spectral characteristics. The collected samples were divided into three subgroups depending on the periodontal health status: periodontitis (P, n = 27), gingivitis (G, n = 23) and healthy elements (H, n = 17). Fig. 2–4 show the median

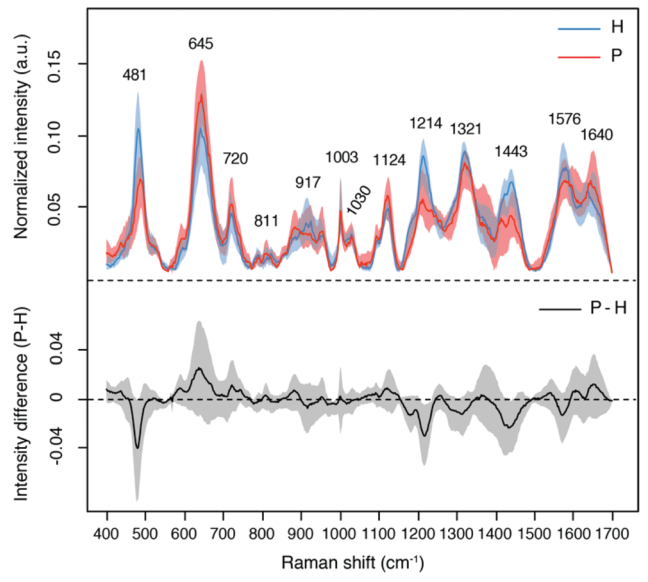

Fig. 2 Comparison of median normalized SERS spectra of GCF collected from healthy dental elements (H, in blue, n = 17), and from elements with periodontitis (P, in red, n = 27), together with their difference spectrum (in black). The corresponding interquartile distributions are represented by the shaded area.

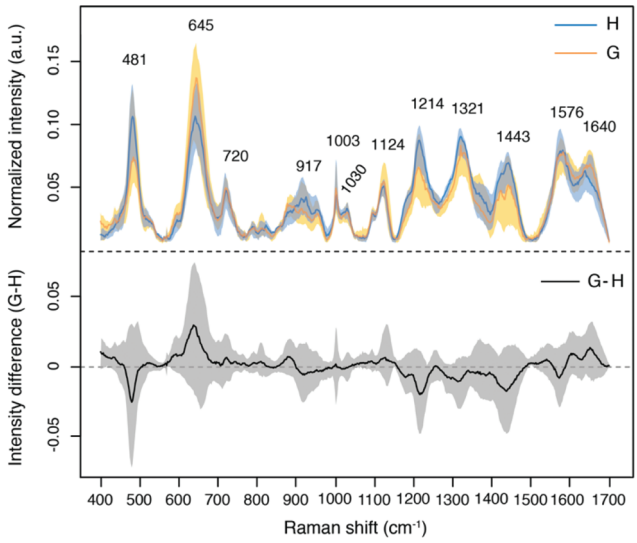

Fig. 3 Comparison of median normalized SERS spectra of GCF collected from healthy dental elements (H, in blue, n = 17) and from elements with gingivitis (G, in orange, n = 23), together with their difference spectrum (in black). The corresponding interquartile distributions are represented by the shaded area.

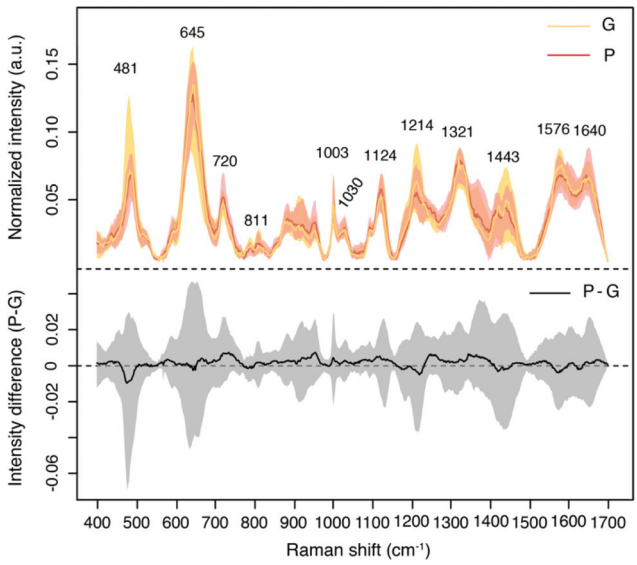

Fig. 4 Comparison of median normalized SERS spectra of GCF collected from elements with periodontitis (P, in red, n = 27) and with gingivitis (G, in orange, n = 23), together with their difference spectrum (in black). The corresponding interquartile distributions are represented by the shaded area.

profile of the SERS spectra aggregated by the diagnosis group, along with their median difference spectra and the corresponding interquartile range (IQR) distributions overlying as shaded colour fills. The overall median profiles are consistent between the groups, with the prominent SERS bands located at around 481, 645, 720, 1003, 1030, 1124, 1214, 1321, 1443, 1576, and 1640 cm^{-1} clearly observed for each group, reflecting the overall GCF composition as detected by SERS. In spite of the similarities, the differences between the spectra of each group are evident. Compared with the SERS spectra of the H group (Fig. 2), the SERS spectra of P samples had higher intensities at 481, 1214, and 1443 cm^{-1} and lower intensities at 645 cm^{-1}. Similarly, comparing the median SERS spectra between the G and the H group (Fig. 3), it is easy to find that the SERS spectra of G samples had higher intensities at 645 cm^{-1} and had lower intensities at 481, 1214, and 1443 cm^{-1}. Furthermore, no substantial differences were observed between the median SERS spectra of the P and G groups (Fig. 4). A comparison of the SERS spectral intensities of GCF between the groups could be made more clearly by looking at the (median) difference spectra. Difference spectra matrices were created by subtracting every spectrum of a selected group (*e.g.* H group) from every spectrum of another group (*e.g.* P group). Positive bands in the resulting median difference spectrum P–H are interpreted as being more abundant in P samples, whereas negative bands are more abundant in H samples. When the IQR shaded area for the difference spectrum did not span a zero line, we accepted the difference as significant. From this point of view, the most significant differences were spotted at 481, 1214 and 1443 cm^{-1} in the P–H difference spectrum. Interestingly, the same pattern can be appreciated also in the G–H spectrum, even though with lower significance. No significant differences were observed between the P and the G groups. According to the tentative spectral interpretation presented above, significant spectral differences between the GCF samples of the three groups could be ascribed to the alterations in the relative concentrations of ergothioneine (relatively higher for H), with less significant contributions from uric acid and hypoxanthine (relatively higher for P and G). Ergothioneine is a dietary amino acid present in many biofluids,[41] where it acts as a strong antioxidant with a putative vitamin-like role.[42] It has been shown that ergothioneine is often highly concentrated at sites of tissue injury; however, a decrease of ergothioneine levels has also been reported for some diseases.[42] Its presence in the SERS spectrum of GCF is documented here for the first time. Much evidence has shown that periodontal inflammation is closely associated with oxidative stress and oxidative stress is known to trigger the chronic state of periodontitis, as evidenced by an increase in biomarker levels for tissue damage. The lack of antioxidant molecules and the excess of reactive oxygen species can be explained as an imbalance of the redox state.[38,43,44] Uric acid is the main antioxidant in saliva[45] and the end product of the purine degradation pathway, a major biochemical source for reactive oxygen species (ROS) production. Hypoxanthine is a metabolic precursor of uric acid in the same degradation pathway. GSH, which is known to have powerful anti-inflammatory and antioxidant activities, is normally present in GCF at concentrations (0.5–2.5 mM) three orders of magnitude higher than the ones normally detected within extracellular tissue compartments (0.5–5 μM in human plasma).[46]

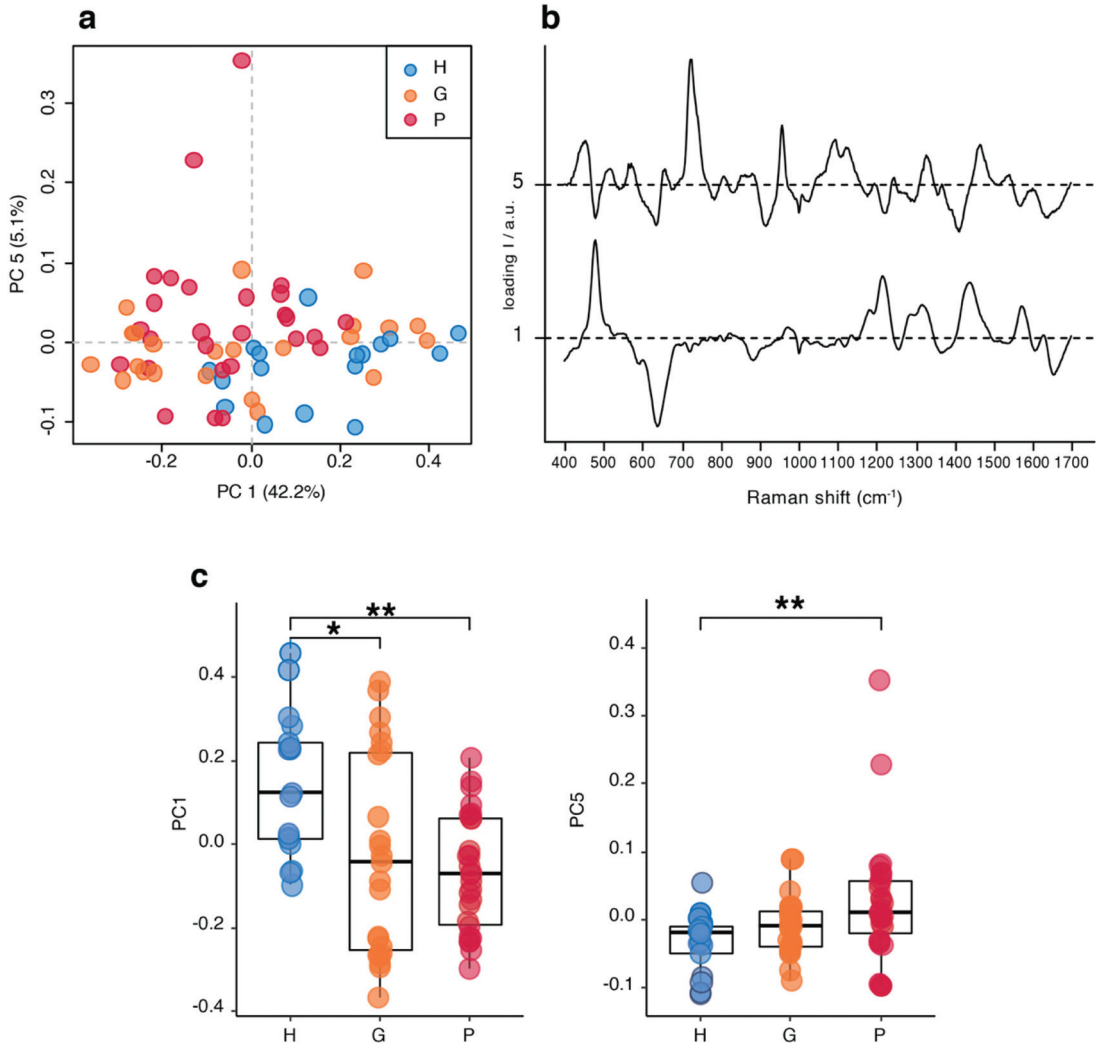

Fig. 5 (a) Score plot of the first principal component (PC1) against the fifth principal component (PC5). Data points (corresponding to single spectra) are depicted with different colours according to the diagnosis (healthy dental elements, H, blue; periodontitis, P, red; gingivitis, G, orange). The data variance (%) explained by each PC is shown between parentheses for both PC1 and PC5. (b) Loadings for the first and fifth principal components. (c) Box plot for the scores on PC1 and PC5. The black line represents the median; the top and bottom edges of the box are the upper and lower quartiles, whiskers extend to upper and lower quartiles plus and minus 1.5× the IQR. The Kruskal–Wallis test with the Dunn–Bonferroni correction for the multiple comparison test (confidence level 95%, * = $p < 0.05$, ** = $p < 0.01$) reveals a significant difference between the H group and the other two groups.

To confirm the spectral differences within the three considered groups, principal component analysis (PCA) was applied as an unsupervised exploratory method, and the results are shown in Fig. 5a–c. PCA is a bilinear decomposition technique, able to reduce large amounts of data into a few parameters, called principal components (PCs), which capture the levels, differences and similarities among the samples and variables constituting the modelled data. This task is achieved by a linear transformation under the constraints of preserving data variance and imposing the orthogonality of the PCs.[47] The first six principal components (covering more than 90% of the total variance) were investigated and the distribution of the score values was visualized. For the sake of conciseness, only the most explanatory results are shown (for a complete depiction, see ESI Fig. S3–5†). Fig. 3A shows the score plot in the plane of the first and fifth principal components (covering about 47% of the total variance) and provides a measure for the clustering of samples. No clear separation of samples according to the three considered groups can be observed. However, it is possible to note how the points corresponding to P and G samples were grouped predominantly in the second and third quadrants (negative score values of PC1), while H samples were grouped predominantly in the fourth quadrant (positive values for PC1 and negative values for PC5). Moreover, it is also possible to note (see ESI Fig. S2†) how samples from the same patient but belonging to distinct diagnosis groups rarely clustered together in the variance space, confirming that the SERS fingerprint of GCF allows the observation of the phenomena localized at the dental element level rather than at the whole oral cavity. Loadings (Fig. 3B) illus-

trate which spectral variables (wavenumbers) were mainly involved in the sample distribution in the principal component space. The samples located at positive values of PC1 (most of the samples of the H group) were characterized by higher positive values for the spectral variables at around 481, 1214 and 1443 cm^{-1}, recognized as the ergothioneine contribution, as well by lower negative values for the band at around 645 cm^{-1}, recognized as the uric acid contribution. Interestingly, loadings on PC1 looked very similar to the median difference spectrum between P and H, and G and H groups, confirming that the main differences between the healthy and the diseased status lie in the relative intensity of the uric acid band at 645 cm^{-1}, lower in the spectra of the diseased samples and the ergothioneine bands, and higher in the healthy elements. On the other hand, the PC5 loadings were mostly inherent to the band at 720 cm^{-1}, where the hypoxanthine contribution can be found. Taking all aspects into consideration, it is easy to spot in the P and G groups the metabolic signature of an accelerated metabolic flux of the purine degradation pathway: the up-regulation of hypoxanthine and the simultaneous decrease in uric acid (as well as other antioxidants, such as ergothioneine) levels at the disease sites. Moreover, two samples seem to reveal a very high hypoxanthine contribution (very high score values for PC5). Because GCF composition is considered to be indicative of the episodic nature of periodontal disease progression and the various stages of inflammation,[48] we possibly related these samples to an "acute" status of inflammation or an aggressive version of periodontitis. Clinical data confirmed the information suggested by PCA: both elements showed severe gingival bleeding on probing (a clinical sign of inflammation), the presence of supragingival plaque and furcation involvement, together with the loss of clinical attachment levels and the sign of a deep periodontal pocket. On the other hand, one sample in the G group exhibited a SERS fingerprint very close to the "healthy" condition. Also for this element, clinical data seem to confirm the information suggested by PCA: this element showed the absence of plaque and a localized mild bleeding to the probe at isolated sites.

Conclusions

Repeatable and stable SERS spectra of gingival crevicular fluid (GCF), which are characteristic of one dental element, can be directly obtained from paper strips using an easy and quick sample preparation. The dominant features in the SERS spectrum of GCF can be ascribed to very few metabolites, in particular to uric acid, hypoxanthine, glutathione and ergothioneine. Moreover, our results revealed that SERS can detect the changes in the GCF compositions between healthy dental elements and elements with periodontal disease, suggesting the promising potential of this technique for developing new modalities in periodontal disease diagnosis, prognosis and surveillance. Further studies that extend this approach to larger cohorts of samples and possibly in combination with multiple analytical platforms are thus required to validate these preliminary results.

CRediT authorship contribution

Stefano Fornasaro: Investigation, conceptualization, methodology, visualization, formal analysis, writing – original draft. Writing – review and editing. Federico Berton: Conceptualization, project administration, writing – review and editing. Claudio Stacchi: Supervision, writing – review and editing. Federica Farina: Investigation and data curation. Alessandro Esposito: Investigation. Valter Sergo: Resources, writing – review and editing. Roberto Di Lenarda: Supervision, resources, funding acquisition, writing – review and editing. Alois Bonifacio: Conceptualization, methodology, visualization, writing – original draft, writing – review and editing.

Conflicts of interest

There are no conflicts to declare.

References

1 G. Bevelander and H. Nakahara, *Anat. Rec.*, 1968, **162**, 313–325.
2 R. R. Wassall and P. M. Preshaw, *Periodontol 2000*, 2016, **70**, 65–79.
3 L. Balducci, A. Ramachandran, J. Hao, K. Narayanan, C. Evans and A. George, *Arch. Oral Biol.*, 2007, **52**, 203–208.
4 V. Nicolin, F. Costantinides, E. Vettori, F. Berton, G. Marchesi, R. Rizzo and R. Di Lenarda, *Clin. Rev. Bone Miner. Metab.*, 2020, **18**, 43–49.
5 P. Papagerakis, L. Zheng, D. Kim, R. Said, A. A. Ehlert, K. K. M. Chung and S. Papagerakis, in *Odontogenesis. Methods in molecular biology*, Humana Press, New York, NY, 2019, vol. 1922, pp. 549–1562.
6 K. Gawron, W. Wojtowicz, K. Łazarz-Bartyzel, A. Łamasz, B. Qasem, P. Mydel, M. Chomyszyn-Gajewska, J. Potempa and P. Mlynarz, *In Vivo*, 2019, **33**, 1165–1174.
7 J. Pei, F. Li, Y. Xie, J. Liu, T. Yu and X. Feng, *EPMA J.*, 2020, **11**, 197–215.
8 W. B. Clark and H. Löe, *Periodontol 2000*, 1993, **2**, 72–82.
9 L. J. Brown and H. Löe, *Periodontol 2000*, 1993, **2**, 57–71.
10 J. G. Caton, G. Armitage, T. Berglundh, I. L. C. Chapple, S. Jepsen, K. S. Kornman, B. L. Mealey, P. N. Papapanou, M. Sanz and M. S. Tonetti, *J. Clin. Periodontol.*, 2018, **45**, S1–S8.
11 I. L. C. Chapple, B. L. Mealey, T. E. Van Dyke, P. M. Bartold, H. Dommisch, P. Eickholz, M. L. Geisinger, R. J. Genco, M. Glogauer, M. Goldstein, T. J. Griffin, P. Holmstrup, G. K. Johnson, Y. Kapila, N. P. Lang, J. Meyle, S. Murakami, J. Plemons, G. A. Romito, L. Shapira, D. N. Tatakis, W. Teughels, L. Trombelli, C. Walter, G. Wimmer,

P. Xenoudi and H. Yoshie, *J. Clin. Periodontol.*, 2018, **45**, S68–S77.
12 M. Ozeki, T. Nozaki, J. Aoki, T. Bamba, K. R. Jensen, S. Murakami and M. Toyoda, *Mass Spectrom.*, 2016, **5**, A0047.
13 H. W. Chen, W. Zhou, Y. Liao, S. C. Hu, T. L. Chen and Z. C. Song, *J. Periodontal Res.*, 2018, **53**, 894–901.
14 A. Bonifacio, in *Nanomaterials for Theranostics and Tissue Engineering*, Elsevier, 2020, pp. 137–174.
15 J. Langer, D. Jimenez de Aberasturi, J. Aizpurua, R. A. Alvarez-Puebla, B. Auguié, J. J. Baumberg, G. C. Bazan, S. E. J. Bell, A. Boisen, A. G. Brolo, J. Choo, D. Cialla-May, V. Deckert, L. Fabris, K. Faulds, F. J. García de Abajo, R. Goodacre, D. Graham, A. J. Haes, C. L. Haynes, C. Huck, T. Itoh, M. Käll, J. Kneipp, N. A. Kotov, H. Kuang, E. C. Le Ru, H. K. Lee, J.-F. Li, X. Y. Ling, S. A. Maier, T. Mayerhöfer, M. Moskovits, K. Murakoshi, J.-M. Nam, S. Nie, Y. Ozaki, I. Pastoriza-Santos, J. Perez-Juste, J. Popp, A. Pucci, S. Reich, B. Ren, G. C. Schatz, T. Shegai, S. Schlücker, L.-L. Tay, K. G. Thomas, Z.-Q. Tian, R. P. Van Duyne, T. Vo-Dinh, Y. Wang, K. A. Willets, C. Xu, H. Xu, Y. Xu, Y. S. Yamamoto, B. Zhao and L. M. Liz-Marzán, *ACS Nano*, 2020, **14**, 28–117.
16 R. Goodacre, M. J. Baker, D. Graham, Z. D. Schultz, M. Diem, M. P. Marques, G. Cinque, R. Vernooij, J. Sulé-Suso, H. J. Byrne, K. Faulds, M. Hermes, H. Fleming, A. Bonifacio, R. Dluhy, P. Gardner, S. El-Mashtoly, B. Wood, K. Gough, S. Fornasaro, S. Kazarian, L. Jamieson, W. Petrich, G. D. Sockalingum, N. Stone, C. Kendall, F. Sinjab, P. Haris, A. Subaihi, S. Remiszewski, P. Hellwig, V. Sergo, K. Gerwert, C. Phillips and C. J. Campbell, *Faraday Discuss.*, 2016, **187**, 575–601.
17 Y. Hong, Y. Li, L. Huang, W. He, S. Wang, C. Wang, G. Zhou, Y. Chen, X. Zhou, Y. Huang, W. Huang, T. Gong and Z. Zhou, *J. Biophotonics*, 2020, **13**, e201960176.
18 S. Cervo, E. Mansutti, G. Del Mistro, R. Spizzo, A. Colombatti, A. Steffan, V. Sergo and A. Bonifacio, *Anal. Bioanal. Chem.*, 2015, **407**, 7503–7509.
19 H. Ito, H. Inoue, K. Hasegawa, Y. Hasegawa, T. Shimizu, S. Kimura, M. Onimaru, H. Ikeda and S. Kudo, *Nanomedicine*, 2014, **10**, 599–608.
20 E. Gurian, P. Giraudi, N. Rosso, C. Tiribelli, D. Bonazza, F. Zanconati, M. Giuricin, S. Palmisano, N. de Manzini, V. Sergo and A. Bonifacio, *Anal. Chim. Acta*, 2020, **1110**, 190–198.
21 S. Feng, R. Chen, J. Lin, J. Pan, G. Chen, Y. Li, M. Cheng, Z. Huang, J. Chen and H. Zeng, *Biosens. Bioelectron.*, 2010, **25**, 2414–2419.
22 A. Stefancu, M. Badarinza, V. Moisoiu, S. D. Iancu, O. Serban, N. Leopold and D. Fodor, *Anal. Bioanal. Chem.*, 2019, **411**, 5877–5883.
23 F. d'Apuzzo, L. Perillo, I. Delfino and M. Portaccio, *J. Biomed. Opt.*, 2017, **22**, 1.
24 P. C. Lee and D. Meisel, *J. Phys. Chem.*, 1982, **86**, 3391–3395.
25 N. Lang, P. M. Bartold, M. Cullinan, M. Jeffcoat, A. Mombelli, S. Murakami, R. Page, P. Papapanou, M. Tonetti and T. V. Dyke, *Ann. Periodontol.*, 1999, **4**, 53–53.
26 N. Lang, W. A. Soskolne, G. Greenstein, D. Cochran, E. Corbet, H. X. Meng, M. Newman, M. J. Novak and H. Tenenbaum, *Ann. Periodontol.*, 1999, **4**, 78–78.
27 J. Lindhe, R. Ranney, I. Lamster, A. Charles, C.-P. Chung, T. Flemmig, D. Kinane, M. Listgarten, H. Löe, R. Schoor, G. Seymour and M. Somerman, *Ann. Periodontol.*, 1999, **4**, 38–38.
28 C. Beleites and V. Sergo, hyperSpec: a package to handle hyperspectral data sets in R, R package version 0.99-20200527, https://cbeleites.github.io/hyperSpec.
29 K. H. Liland, T. Almøy and B.-H. Mevik, *Appl. Spectrosc.*, 2010, **64**, 1007–1016.
30 B. R. Lutz, C. E. Dentinger, L. N. Nguyen, L. Sun, J. Zhang, A. N. Allen, S. Chan and B. S. Knudsen, *ACS Nano*, 2008, **2**, 2306–2314.
31 W. E. Doering, M. E. Piotti, M. J. Natan and R. G. Freeman, *Adv. Mater.*, 2007, **19**, 3100–3108.
32 A. Bonifacio, S. Dalla Marta, R. Spizzo, S. Cervo, A. Steffan, A. Colombatti and V. Sergo, *Anal. Bioanal. Chem.*, 2014, **406**, 2355–2365.
33 W. R. Premasiri, J. C. Lee and L. D. Ziegler, *J. Phys. Chem. B*, 2012, **116**, 9376–9386.
34 P. Hu, X.-S. Zheng, C. Zong, M.-H. Li, L.-Y. Zhang, W. Li and B. Ren, *J. Raman Spectrosc.*, 2014, **45**, 565–573.
35 S. Stewart and P. M. Fredericks, *Spectrochim. Acta, Part A*, 1999, **55**, 1615–1640.
36 C. M. Silva-Boghossian, A. P. V. Colombo, M. Tanaka, C. Rayo, Y. Xiao and W. L. Siqueira, *PLoS One*, 2013, **8**, e75898.
37 P. Tripathi, V. Blaggana, P. Upadhyay, M. Jindal, S. Gupta and S. Nishat, *J. Indian Soc. Periodontol.*, 2019, **23**, 25.
38 S. Narendra, U. K. Das, S. K. Tripathy and N. C. Sahani, *J. Contemp. Dent. Pract.*, 2018, **19**, 874–880.
39 V. M. Barnes, R. Teles, H. M. Trivedi, W. Devizio, T. Xu, M. W. Mitchell, M. V. Milburn and L. Guo, *J. Dent. Res.*, 2009, **88**, 851–855.
40 G. Campisciano, A. Toschetti, M. Comar, R. D. Taranto, F. Berton and C. Stacchi, *Eur. J. Dent*, 2017, **11**, 126–129.
41 S. Fornasaro, E. Gurian, S. Pagarin, E. Genova, G. Stocco, G. Decorti, V. Sergo and A. Bonifacio, *Spectrochim. Acta, Part A*, 2021, **246**, 119024.
42 I. Borodina, L. C. Kenny, C. M. McCarthy, K. Paramasivan, E. Pretorius, T. J. Roberts, S. A. van der Hoek and D. B. Kell, *Nutr. Res. Rev.*, 2020, 1–28.
43 E. Baltacıoğlu, P. Yuva, G. Aydın, A. Alver, C. Kahraman, E. Karabulut and F. A. Akalın, *J. Periodontol.*, 2014, **85**, 1432–1441.
44 A. Gustafsson and B. Asman, *J. Clin. Periodontol.*, 1996, **23**, 38–44.
45 I. Peluso and A. Raguzzini, *Pathol. Res. Int.*, 2016, **2016**, 1–14.
46 I. L. C. Chapple, G. Brock, C. Eftimiadi and J. B. Matthews, *Mol. Pathol.*, 2002, **55**, 367–373.
47 M. Li Vigni, C. Durante and M. Cocchi, in *Data Handling in Science and Technology*, Elsevier, 2013, vol. 28, pp. 55–126.
48 L. Jin, B. Söder and E. F. Corbet, *J. Periodontol.*, 2000, **71**, 929–939.